Faraday Discussions

Cite this: *Faraday Discuss.*, 2015, **185**, 37

PAPER

Photosynthetic water oxidation: binding and activation of substrate waters for O–O bond formation

David J. Vinyard, Sahr Khan and Gary W. Brudvig*

Received 21st May 2015, Accepted 1st June 2015
DOI: 10.1039/c5fd00087d

Photosynthetic water oxidation occurs at the oxygen-evolving complex (OEC) of Photosystem II (PSII). The OEC, which contains a Mn_4CaO_5 inorganic cluster ligated by oxides, waters and amino-acid residues, cycles through five redox intermediates known as S_i states (i = 0–4). The electronic and structural properties of the transient S_4 intermediate that forms the O–O bond are not well understood. In order to gain insight into how water is activated for O–O bond formation in the S_4 intermediate, we have performed a detailed analysis of S-state dependent substrate water binding kinetics taking into consideration data from Mn coordination complexes. This analysis supports a model in which the substrate waters are both bound as terminal ligands and react *via* a water-nucleophile attack mechanism.

1. Introduction

The climate, biology and geology of Earth were transformed by the evolution of oxygenic photosynthesis approximately three billion years ago.[1] All photosynthetic organisms, from the earliest cyanobacteria to modern vascular plants, use solar energy to oxidize water to molecular oxygen (O_2), protons and electrons at the oxygen-evolving complex (OEC) of Photosystem II (PSII).[2,3] PSII is a membrane-bound pigment–protein complex that generates a solar light-induced charge separation in order to oxidize water and reduce plastoquinone. The charge separation is initiated by the primary chlorophyll-a electron donor, P_{680}, forming a powerful oxidant, P_{680}^+, that advances the oxidation state of the Mn_4CaO_5 cluster in the OEC (Fig. 1) *via* a redox-active tyrosine, Y_Z, that mediates electron transfer from the OEC to P_{680}^+. The overall four-electron process leads to the formation of O_2 that is released as a byproduct and has accumulated in the biosphere and the release of protons that contribute to the *trans*-membrane proton motive force.[4] The availability of O_2 as an electron sink has since powered oxygenic respiration to give rise to Earth's current biological diversity.

Department of Chemistry, Yale University, New Haven, CT, United States. E-mail: gary.brudvig@yale.edu

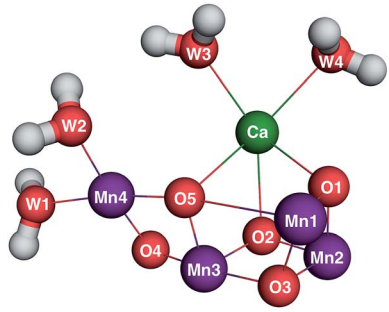

Fig. 1 Quantum mechanics/molecular mechanics (QM/MM) optimized S_1 structure of the OEC[5] based on the 1.9 Å resolution crystal structure by Shen and coworkers.[6]

The catalytic cycle of the OEC involves five metastable redox intermediates known as S_i states ($i = 0$–4), as first described by Kok and coworkers.[7,8] The dark-stable intermediate, S_1, contains the Mn oxidation state pattern (III,IV,IV,III)[9] (order of oxidation states is based on the numbering of the Mn ions in Fig. 1) and is converted to S_2 upon the loss of one electron. S_2 is present as two spin isomers with oxidation states of (III,IV,IV,IV) ($S = 1/2$) or (IV,IV,IV,III) ($S = 5/2$).[10] The next oxidation event results in the loss of one proton and one electron from the OEC to form S_3, in which all four Mn ions are in the +4 oxidation state ($S = 3$).[11,12] Oxidation of Y_Z following the next charge separation causes release of a proton from S_3 to form a modified $Y_Z^{\bullet}$ S_3' state,[13] which then forms the S_4 state. The structures of S_3' and S_4 are poorly understood. S_4 spontaneously produces O_2, binds substrate water(s), and releases a proton to form S_0, thus resetting the catalytic cycle.

The general structure of the OEC has been revealed through a series of X-ray diffraction (XRD) studies.[6,14–17] However, the atomic structure of any single Kok cycle intermediate has not been determined through these experiments. Early XRD structures of the OEC suffered from X-ray induced reduction of the high-valent Mn centers.[18] Nevertheless, the availability of metal–metal distances from extended X-ray absorption fine structure (EXAFS) spectroscopy[19,20] allowed computational studies (QM/MM and density functional theory (DFT)) to refine XRD models to structures corrected for radiation damage.[5,21] At present, the PSII research community is in general (but not universal[3]) agreement on the structures of the S_0,[5] S_1,[5,10] and S_2[10] intermediates and the Mn oxidation states of all S states.[9]

The problem of X-ray induced Mn reduction can be completely avoided by using femtosecond pulses from X-ray free electron laser (XFEL) radiation sources.[22,23] XFEL studies using PSII nanocrystals have produced structures of dark-adapted PSII at 6.5–4.9 Å resolution.[24–27] Structures of S_2,[25,26] S_3,[26,27] and S_0[26] have also been reported at low resolution, which limits their interpretation. However, QM/MM methods combined with electron density map analysis have shown that the $S_1 \rightarrow S_2$ transition involves significant displacement (and oxidation) of Mn4 (also referred to as the "dangler" Mn).[28] A 1.95 Å resolution XFEL structure of dark-adapted PSII was recently reported by Shen and coworkers.[29] However, the resulting XRD model of the OEC does not agree well with EXAFS data of S_1,[19] which is likely the result of inaccuracy in positioning of the bridging oxo ligands and significant accumulation of S_0.[30]

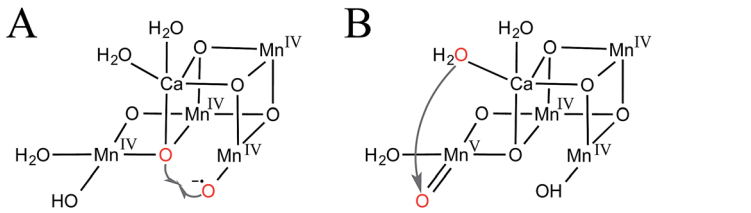

Fig. 2 Proposed mechanisms of O–O bond formation in the S_4 intermediate. (A) Oxo–oxyl radical coupling and (B) water-nucleophile attack. Substrate waters are shown in red.

The S_4 state decays faster than it is formed and, therefore, cannot be observed as a kinetic intermediate. Consequently, no direct experimental evidence for the nature of O–O bond formation in S_4 has been produced. However, insights from inorganic and computational chemistry have produced two competing mechanisms: water-nucleophile attack and oxo–oxyl radical coupling.

In the oxo–oxyl radical coupling mechanism,[31–33] a Mn(IV)–oxyl radical reacts with a Mn-bridging oxo to generate O_2 (Fig. 2A). Extensive calculations by Siegbahn suggest that one of the substrate waters first binds during the $S_2 \rightarrow S_3$ transition and then is oxidized to an oxyl radical in S_4 to carry out the reaction.[32]

A water-nucleophile attack mechanism for the OEC[34–37] is most consistent with synthetic water oxidation catalysts.[38] As shown in Fig. 2B, such a mechanism would involve a terminal water-nucleophile (preferably bound to calcium, see discussion below) and a formally Mn(V)–oxo electrophile.

These mechanisms can be distinguished by the positions of the substrate waters involved. Kinetics of substrate water exchange throughout the Kok cycle have been determined by membrane inlet mass spectrometry (MIMS) measurements following rapid mixing of PSII with $H_2{}^{18}O$. This technique, which was pioneered in the Wydrzynski laboratory, allows $^{34}O_2$ and $^{36}O_2$ release by PSII in specific S states (advanced by single-turnover flashes) to be monitored as a function of incubation time with $H_2{}^{18}O$.[39,40] The resulting rates of substrate water exchange are summarized in Table 1. In S_0, only one slowly exchanging water (W_s) is resolved with a rate constant of approximately 10 s^{-1}. The exchange rate of W_s is then dramatically slowed to 0.02 s^{-1} in S_1. In S_2 and S_3, two phases of substrate water exchange kinetics are resolved; the slower and faster exchanging waters are referred to as W_s and W_f, respectively. W_s exchanges at a nearly identical rate in S_2 and S_3, but the rate is much faster than in S_1. W_f exchanges at decreasing rates in S_1, S_2, and S_3.

Determining the molecular mechanism of photosynthetic water oxidation is crucial for applying the principles of Nature's design to synthetic systems for solar

Table 1 Substrate water exchange rates in spinach thylakoids at 10 °C.[39,41]

	k_s, s^{-1}	k_f, s^{-1}
S_0	~10	>120
S_1	~0.02	>120
S_2	~2	~120
S_3	~2	~40

fuel production. In the following analysis, we detail models for substrate binding and O–O bond formation in the OEC in light of experimental evidence and comparisons to well-studied inorganic systems.

2. Where are the substrate binding sites?

Kinetics and mechanism of terminal water *vs.* μ-oxo ligand exchange from model chemistry

Given our current understanding of the structure of the OEC in the S_0, S_1, and S_2 states, we can predict that the substrate waters that give rise to O_2 are bound either as terminal ligands to Mn4 and Ca^{2+}, or as μ-oxo/hydroxo bridges. In order to understand the substrate water exchange kinetics of the OEC, we first look to inorganic model systems.

The exchange rate of a terminal water ligand on Mn depends greatly on the oxidation state, protonation, ancillary ligands, and geometry. As shown in Table 2, both the water exchange rate and pK_a of a terminal aqua ligand decrease dramatically with increasing oxidation state from Mn^{2+} to Mn^{3+} to Mn^{4+}. The hexaaqua Mn(IV) complex has an especially slow water ligand exchange rate ($<10^{-4}$ s^{-1}), as expected for a high-spin d^3 ion with octahedral geometry for which the ligand field stabilization energy disfavors ligand dissociation leading to very slow ligand exchange. However, exchange of the terminal water ligands of the $[Mn_4^{IV,IV,IV,IV}(\mu\text{-}O)_5(terpy)_4(H_2O)_2]^{6+}$ (terpy = 2,2′:6′,2″-terpyridine) complex occurs faster than the mixing time for the mass spectrometry measurement (~10 s, $k_{ex} > 10^{-1}$ s^{-1}), despite the high-spin d^3 configuration of the Mn(IV) ions. This can be explained by the reduced symmetry of the Mn(IV) ions in the tetrameric oxomanganese–terpy complex. Deviations from octahedral geometry of the Mn^{IV} centers resulting from the <90° bite angle of the tridentate terpy ligand and the asymmetry associated with oxo and pyridyl ligands result in loss of degeneracy of the t_{2g} and e_g orbitals, and can lower the barrier for exchange of the terminal

Table 2 pK_a values and exchange rates of terminal waters. Calculated values appear in italics

	pK_a	Reference	k_{ex}, s^{-1}	Reference
$[Ca(H_2O)_6]^{2+}$	12.8	43	~10^8	44
$[Sr(H_2O)_6]^{2+}$	13.2	43	~10^9	44
$[Mn(H_2O)_6]^{2+}$	10.6	45	2×10^7	46
			1×10^7	47
$[Mn(H_2O)_6]^{3+}$	0.7	45	*2×10^3*	47
			0.01–1	39 and 48
$[Mn(H_2O)_6]^{4+}$	<0		*10^{-6} to 10^{-4}*	39
			10^{-7} to 10^{-8}	48
$[Mn_2^{III,IV}(\mu\text{-}O)_2(mes\text{-}terpy)_2(H_2O)_2]^{3+a}$	nd[d]		>10^{-1}	49
$[Mn_4^{IV,IV,IV,IV}(\mu\text{-}O)_5(terpy)_4(H_2O)_2]^{6+b}$	nd		>10^{-1}	49
$[Mn_2^{IV,IV}(\mu\text{-}O)_2(terpy)_2(H_2O)_2]^{4+}$	1.8	50	nd	
$[Mn_2^{III,III}(L)_2(H_2O)]^{+c}$	19–20	51	nd	
$[Mn_2^{III,IV}(L)_2(H_2O)]^{2+c}$	10–11	51	nd	

[a] mes-terpy = 4′-mesityl-2,2′:6′,2″-terpyridine. [b] terpy = 2,2′:6′,2″-terpyridine. [c] L = 2-hydroxy-1,3-bis(3,5-X_2-salicylideneamino)propane. [d] nd = not determined.

water ligands. Indeed, computational studies have found low reaction barriers for the dissociative exchange of terminal waters in μ-O bridged Mn(IV) dimers.[42]

Generally, ligand exchange for high-valent first-row transition ions involves a dissociative mechanism, especially for Mn(IV) which is normally six-coordinate and has a small ionic radius that makes an associative mechanism unfavorable. For terminal water ligands, dissociation involves removing a polar but neutral ligand from the cationic metal center, which has a modest barrier.[52] However, dissociative exchange of a μ-oxo ligand involves removing an anionic ligand from the cationic metal center, which has a much higher barrier. Therefore, the exchange of μ-oxo ligands with bulk water is thermodynamically more challenging than the exchange of terminal water ligands.

The mechanism of μ-oxo exchange has been investigated for di-μ-oxo di-Mn(III,IV) complexes.[53] These studies have shown that μ-oxo exchange requires protonation of the oxo before dissociation and exchange; therefore, μ-oxo pK_as are good predictors of their rates of exchange. The μ-oxo pK_a decreases dramatically with increasing Mn oxidation state in Mn model complexes (Table 3). The rate of μ-oxo exchange is very fast for Mn(III,III) dimers, owing to the high pK_a of the μ-oxo ligands. Indeed, di-μ-oxo di-Mn(III,III) complexes are generally not stable to hydrolysis. For di-μ-oxo di-Mn(III,IV) complexes, the rate of μ-oxo exchange is on a timescale of minutes ($t_{1/2} = 21$ min for the $[Mn_2^{III,IV}(\mu\text{-}O)_2(bpy)_4]^{3+}$ complex, bpy = 2,2′-bipyridine).[53] However, no μ-oxo exchange could be detected on a one-day timescale for all-Mn(IV) complexes, such as $[Mn_4^{IV,IV,IV,IV}(\mu\text{-}O)_5(terpy)_4(H_2O)_2]^{6+}$, reflecting the very low pK_a of the μ-oxo ligands in all-Mn(IV) complexes (Table 3).

The $[Mn_2^{III,IV}(\mu\text{-}O)_2(terpy)_2(H_2O)_2]^{3+}$ complex contains terminal water ligands adjacent to the μ-oxo ligands. It has been found that the terminal water ligands accelerate the rate of μ-oxo exchange.[53] Because the pK_a of the water ligand bound to a high-valent Mn center is lower than solvent water (Table 2), a μ-oxo can be more readily protonated by ligated water, which opens up the μ-oxo bridge and lowers the energetic barrier for dissociation.[53] In this mechanism, the terminal water and μ-oxo are in dynamic equilibrium with bulk water. For Mn dimers without terminal water ligands, the exchange is much slower, such as in $[Mn_2^{III,IV}(\mu\text{-}O)_2(bpy)_4]^{3+}$, because intramolecular proton transfer between terminal-bound water and μ-oxo bridges is eliminated.[53]

There have also been measurements of terminal water and μ-oxo ligand exchange of the di-Mn center in Mn-catalase.[54] The active site of Mn-catalase contains a redox-active di-Mn center for which ligand exchange has been studied in the di-μ-oxo di-Mn(III,IV) state. It was found that the terminal water ligand exchanges within the mixing time of one minute, but the μ-oxo ligands require over one hour for exchange. These results parallel those obtained for Mn model complexes in solution, although the exchange rate of the μ-oxo ligands is much lower in the protein active site.

Table 3 μ-oxo pK_a values of $[Mn_2(\mu\text{-}O)_2(bpy)_4]^{n+}$. Calculated values appear in italics

	pK_a	Reference
$[Mn_2^{III,III}(\mu\text{-}O)_2(bpy)_4]^{2+}$	*12.4*	55
$[Mn_2^{III,IV}(\mu\text{-}O)_2(bpy)_4]^{3+}$	2.3	49
$[Mn_2^{IV,IV}(\mu\text{-}O)_2(bpy)_4]^{4+}$	*−6.5*	55

In summary, electrostatics play a dominant role in the dissociative ligand exchange reactions of high-valent oxo–manganese complexes. There is a large barrier for μ-oxo exchange due to the high negative charge of the oxo ligand. Thus, protonation of the μ-oxo ligand is required to promote ligand exchange. Because of the large pK_a shift of the μ-oxo ligands between di-μ-oxo di-Mn(III,IV) and di-μ-oxo di-Mn(IV,IV) complexes, μ-oxo ligands exchange at a modest rate for di-μ-oxo di-Mn(III,IV) complexes but do not exchange for di-μ-oxo di-Mn(IV,IV) centers. On the other hand, terminal water ligands exhibit fast rates of ligand exchange for both Mn(III) and Mn(IV) centers. Moreover, the rate of terminal water ligand exchange is similar for Mn(III) and Mn(IV) because both have similar electrostatic potential (ESP) charges.[52]

Ammonia does not compete with substrate water

The water analog ammonia inhibits the OEC by binding to two sites in PSII. The first is in the outer coordination sphere of the OEC and upon binding of ammonia, alters the hydrogen-bonding networks in such a way that the S_2 state $S = 5/2$ isomer is favored.[56] The binding of ammonia to this site is competitive with chloride[57,58] and can be accessed by larger amines,[56,58] but its specific location has not been resolved.

Ammonia also binds directly to Mn in the OEC in the S_2 state resulting in the formation of an altered multiline $g = 2$ EPR signal.[59] However, the substrate water exchange kinetics of S_2 do not change when ammonia is bound.[60] Therefore, the binding site of ammonia *cannot* be the binding site of a substrate water.

Lubitz and coworkers have proposed that ammonia binds to Mn4 *trans* to O5 based on ^{17}O-ELDOR-detected NMR (EDNMR) measurements.[60] In these experiments, dark-adapted PSII (poised in S_1) is incubated with $H_2{}^{17}O$ for tens of minutes and perturbations in the ^{17}O-EDNMR signal are detected when ammonia (as NH_4Cl at pH 7.6) is present following advancement to the S_2 state by 200 K illumination and subsequent annealing at 260 K. In accompanying ^{1}H-ENDOR measurements, no change in the proton environment around the OEC was observed.[60]

Other lines of evidence have suggested that ammonia binds as a bridging ligand between two Mn ions. This motif was first proposed by Britt and coworkers based on ESEEM measurements of the ammonia-bound S_2 state in higher plant PSII.[61] The quadrupole coupling between the $S = 1/2$ S_2 state of the OEC and bound $^{14}NH_3$ was resolved as 1.61 MHz with $\eta = 0.59$. A very similar coupling was observed in cyanobacterial PSII (1.52 MHz, $\eta = 0.47$).[60] For comparison, a nitrogen nucleus with purely axial symmetry is characterized by $\eta = 0$, while ammonia

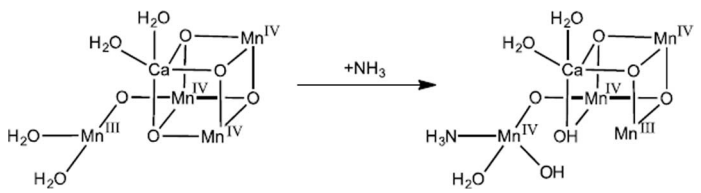

Fig. 3 Proposed mechanism of ammonia binding in the S_2 intermediate. Ammonia binds as an additional ligand to the dangler Mn in the $S = 5/2$ S_2 state, which induces a redox switch to the $S = 1/2$ state. Adapted from ref. 63.

(amino) ligands display $\eta \leq 0.3$. Therefore, the measured quadrupole coupling of ammonia to S_2 is highly deviant from axial symmetry and could represent a deprotonated bridging ligand such as an imido (NH^{2-}) or nitrido (N^{3-}). However, Britt and coworkers have very recently revealed the origin of this anisotropy. In wild type cyanobacterial PSII, they measured the $^{14}NH_3$ coupling as 1.62 MHz with $\eta = 0.40$, but in a D1-D61A mutant, the interaction was nearly completely axial (1.54 MHz, $\eta = 0.04$).[62] This work provides convincing evidence that bound ammonia has a strong hydrogen bond to Asp61 and is, therefore, a terminal ligand to Mn4.

In a recent study using QM/MM methods and EXAFS simulations, we have proposed that instead of replacing a terminal water or μ-oxo group, ammonia binds as a sixth ligand to Mn4 resulting in a complete octahedral coordination sphere.[63] In this model (Fig. 3), ammonia binds to the $S = 5/2$ S_2 state but then induces a redox switch stabilizing the $S = 1/2$ S_2 state by protonating O5 and deprotonating W2. This additional ligand would lower the reduction potential of ammonia-bound S_2 as has been observed by both thermoluminescence[64] and flash O_2 measurements.[65]

While both substrate waters are already bound in S_2,[41] an additional water may bind during the $S_2 \rightarrow S_3$ transition as computationally predicted.[32] We have proposed that ammonia, a "harder" Lewis base than water, binds in S_2 to the dangler Mn4 in an analogous site as water binds in S_3 to the dangler Mn4.[63] The addition of a ligand to Mn4 in either S_2 or S_3 *trans* to O5 would cause the other terminal water ligands (W1 and W2) to shift their positions towards the cuboidal core of the OEC. In this model of ammonia binding, both water–nucleophile attack and oxo–oxyl radical coupling O–O bond formation mechanisms are feasible.

A model for substrate water exchange in the OEC

W2 exchanges rapidly. In agreement with previous analyses,[66,67] we assign the kinetic features of W_f primarily to the terminal water W2. This water is already bound in S_2 as resolved in measurements at reduced temperatures[41] and in PSII cores from the red alga *Cyanidioschyzon merolae*.[68] In S_0 and S_1, W2 is present as a Mn^{3+}-aqua species and would be rapidly exchanged (>120 s^{-1}), consistent with the predicted exchange kinetics of $[Mn(H_2O)_6]^{3+}$ (Fig. 4, Table 2).

For the water-nucleophile attack mechanism, the substrate waters are W2 and W3. W3, which is bound to Ca^{2+}, is also expected to exchange rapidly (specifically in S_0 and S_1, see discussion below). Therefore, the W_f kinetic (measured by monitoring $^{34}O_2$) may reflect contributions from both W2 and W3.

The exchange rate of W2 is first resolved after the $S_1 \rightarrow S_2$ transition with a value in the S_2 state of $k_f \sim 120$ s^{-1}. As discussed above, S_2 is present as two spin isomers. Given the changes seen in XFEL experiments at the Mn4 position measured at physiological temperature, we have asserted that the $S = 1/2$ isomer is dominant.[28] Therefore, W_f would be bound as a terminal Mn^{4+}-aqua species in the S_2 state and exchanges at a rate comparable to those measured in model complexes (Table 2).

As modeled in Fig. 4, the formation of S_3 involves the release of a proton from W2 and a 3-fold slowing of its exchange rate (Table 1). This change is qualitatively consistent with the differences expected between Mn^{4+}-aqua and Mn^{4+}-hydroxo species.

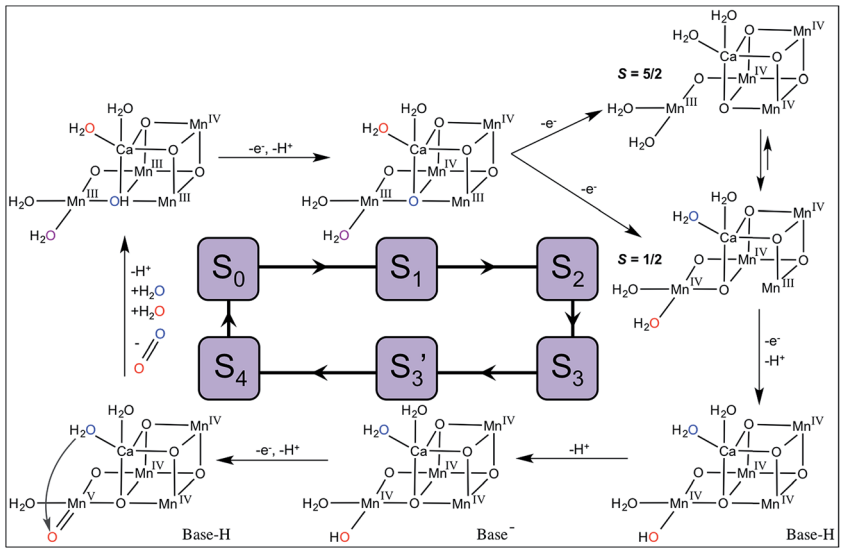

Fig. 4 Proposed mechanism of OEC turnover and substrate water exchange. W_s is shown in blue and W_f in red (in S_0 and S_1, W2 is shown in purple as it contributes to both the W_s and W_f kinetics).

W_s in S_0 and S_1 involves O5/W2 exchange. Identifying the origin of the substrate water exchange rates for the W_s kinetic phase is more complex. The water exchanges fastest in S_0, dramatically slows down in S_1, and then dramatically speeds up again in S_2 and S_3. These observations are difficult to explain based on exchange at a single site. Herein, we propose a new model for W_s exchange that involves contributions from both terminal and bridging ligands (W2 and O5, respectively) whose interconversion is possible only in the S_0 and S_1 states owing to the decreasing pK_a of the μ-oxo species, O5, with increasing Mn oxidation states.

It has been determined that only one of the μ-oxo bridges denoted O5 slowly exchanges with $H_2{}^{17}O$ in the dark-stable S_1 state over tens of seconds.[54,69] We assume that O5 also exchanges with bulk water in S_0 (oxidation states III,IV,III,III). QM/MM models of the S_0 state[5] predict that O5 is protonated, as expected if its pK_a is compared to Mn(III,III) dimers (Table 3). Consequently, O5 exchange would be expected to occur relatively rapidly in S_0 (10 s^{-1}) because it is already protonated at physiological pH. During exchange, protonated O5 may dissociate from Mn3 becoming a terminal water ligand to Mn4. Thus, in the S_0 state, W2 (purple, Fig. 4) and O5 (blue, Fig. 4) are expected to be in rapid equilibrium with each other.

In S_1 (oxidation states III,IV,IV,III), O5 is present in a chemical environment analogous to Mn(III,IV) dimer complexes and the pK_a of O5 in S_1 is predicted to be much lower than in S_0 (Table 3). Based on QM/MM models, O5 is not protonated in the S_1 state[5,21] and, thus, would have a higher energetic barrier for exchange. This change is proposed to be the reason for the 500-fold decrease in the exchange rate of W_s observed in S_1 as compared to S_0.

W_f is not resolved in S_0 and S_1 and reflects the rapid exchange of W2 (and W3, discussed below). Because μ-oxo exchange involves subsequent dissociation, binding, and association steps,[53] isotopically labeled substrate will appear in both the O5 and W2 positions. Therefore, W2 is labeled with two rates. The first is rapid (>120 s^{-1}) and reflects direct exchange with bulk water. The second kinetic is slow (0.02–10 s^{-1}) and reflects the interconversion of labeled O5 with W2. *Crucially, this mechanism implies that the rate of W_s exchange is controlled by the rate of O5 exchange in S_0 and S_1, but that O5 is not necessarily a substrate water.*

For the dominant S_2 state $S = 1/2$ spin isomer (oxidation states IV,IV,IV,III), the O5 chemical environment is analogous to Mn(IV,IV) dimer complexes in which the μ-oxo pK_a is very low (Table 3). Given the large energetic barrier for μ-oxo exchange, the measured rate of W_s in S_2 (2 s^{-1}) is too fast to be assigned to O5.

W_s in S_2 and S_3 involves a terminal water bound to Ca^{2+}. In S_0 and S_1, W3, which is a substrate water in the proposed water-nucleophile attack mechanism (Fig. 2B and 4), exchanges at a rate >120 s^{-1} and its kinetic features are merged with those of W2. However, the $S_1 \rightarrow S_2$ transition does not involve the release of a proton to the bulk, but does involve an oxidation. The result is the build-up of a positive charge and a significant contraction of the OEC as recently observed in photothermal beam deflection experiments.[13,70] This accumulated charge (and contraction) is not released until the S_0 state is reformed after O_2 release.[70] As a result, we hypothesize that the Ca^{2+}–W3 electrostatic interaction, as well as the surrounding hydrogen-bonding network, is stronger in S_2 and S_3 compared to S_0 and S_1. This effect of the increased charge would have to be dramatic to explain the 10^6-fold decrease in W3 exchange compared to the Ca^{2+}-aqua ion in bulk water (Table 2).

When Ca^{2+} is substituted with Sr^{2+}, only W_s is significantly affected: k_s is three- to four-fold faster in S_1, S_2, and S_3 when Sr^{2+} is present.[71] Both O5 and W3 are adjacent to Ca^{2+}/Sr^{2+} and are, therefore, reasonable candidates for W_s. Because Ca^{2+} and Sr^{2+} have very similar Lewis acidities (similar pK_as of the aqua ion, Table 2), W3 is expected to be fully protonated throughout the Kok cycle providing an adequate nucleophile in the water-nucleophile attack mechanism.[36] However, Sr^{2+} is considerably larger than Ca^{2+} (ionic radii are 1.12 Å and 0.99 Å, respectively[72]) resulting in a weaker electrostatic interaction between Sr^{2+} and its ligands. This difference is reflected in the faster exchange rate of the water ligands bound to $[Sr(H_2O)_6]^{2+}$ compared to $[Ca(H_2O)_6]^{2+}$ (Table 2), and is also consistent with the faster exchange of W_s when Sr^{2+} is substituted for Ca^{2+} in the OEC.

In our model for OEC turnover and substrate water exchange shown in Fig. 4, the observed W_s kinetics reflect O5 exchanging with W2 in S_0 and S_1, and W3 exchange in S_2 and S_3. The W_f kinetic reflects both W2 and W3 exchange in S_0 and S_1, and only W2 in S_2 and S_3. This new substrate exchange model provides a complete description of all of the kinetic phases of substrate exchange throughout the S-state cycle and is consistent with data from model high-valent oxomanganese complexes. It, thus, provides a framework from which to design additional experimental measurements to test and validate this hypothesis.

3. Mechanism of O–O bond formation

The structure of the S_4 intermediate will determine if the mechanism of photosynthetic water oxidation involves water-nucleophile attack or oxo–oxyl radical

coupling. Unfortunately, few experimental clues about S_4 are available. Given that the Mn oxidation states in S_3 are (IV,IV,IV,IV), the S_4 state is predicted to contain either a Mn^{IV}–oxyl radical or Mn^{V}–oxo species.

A Mn^{IV}–oxyl radical species has been suggested through computational studies by Siegbahn and supports an oxo–oxyl radical coupling mechanism. On the other hand, a high-spin Mn^{V}–oxo is predicted to serve as the electrophile in a water-nucleophile attack mechanism. Borovik and coworkers have recently reported experimental support for the latter option through studies of $[Mn^{V}H_3buea(O)]$ (where buea = tris[(*N*′-*tert*-butylureaylato)-*N*-ethylene]aminato).[73,74] The buea ligand imposes C_3 symmetry around Mn and stabilizes the Mn–oxo group through intramolecular hydrogen bonding. $[Mn^{V}H_3buea(O)]$ is a high-spin $S = 1$ system as confirmed by EPR spectroscopy and supported by DFT calculations.[73] Therefore, the d_{xz} and d_{yz} orbitals in $[Mn^{V}H_3buea(O)]$ are degenerate and the Mn–oxo bond is likely to be weaker (and more reactive) than corresponding Mn^{V}–oxo species with tetragonal symmetry ($S = 0$). By quantifying the hyperfine contributions from ^{17}O-labeled $[Mn^{V}H_3buea(O)]$ using EPR spectroscopy, Borovik and coworkers determined that 0.45 spins reside on the oxo group. Therefore, the Mn^{V}–oxo group is strongly covalent, but does not contain an oxyl radical. For $[Mn^{III}H_3buea(O)]^{2-}$, only 0.30 spins reside on the oxo group, suggesting that the Mn–O bond becomes more strongly covalent (and the unit more electrophilic) with increasing Mn oxidation state.[74]

To date, no experimental evidence of a Mn^{IV}–oxyl radical species has been found, calling into question the accuracy of the oxo–oxyl radical coupling mechanism. However, if a reactive high-spin Mn^{V}=O species is present in the S_4 state, analogous to that found in $[Mn^{V}H_3buea(O)]$, a water-nucleophile attack mechanism would lead to O–O bond formation.

4. Conclusions

Determining the molecular mechanism of O–O bond formation in photosynthetic water oxidation remains one of the great challenges in bioinorganic chemistry. In the absence of direct experimental evidence of the S_4 intermediate, we can predict its structure and, therefore, the mechanism of O–O bond formation by comparing the OEC to model Mn complexes and by determining where the substrate waters bind throughout the catalytic cycle.

In our proposed model of OEC turnover shown in Fig. 4, the substrate waters are W2 (terminal water on Mn4) and W3 (terminal water on Ca^{2+}). The substrate water exchange kinetics in S_0 and S_1 are complicated by the dynamic equilibrium between W2 and the slowly exchanging μ-oxo/hydroxo bridge, O5. This assignment of substrates dictates that O–O bond formation occurs *via* a water-nucleophilic attack of W3 (as water) on W2 (as a high-spin Mn^{V}=O species).

Acknowledgements

Funded by the U.S. Department of Energy, Office of Science, Office of Basic Energy Sciences (Grant no. DE-FG02-05ER15646). We thank Mikhail Askerka and Dr. Leslie Vogt for helpful discussions.

References

1 S. A. Crowe, L. N. Dossing, N. J. Beukes, M. Bau, S. J. Kruger, R. Frei and D. E. Canfield, *Nature*, 2013, **501**, 535–538.
2 J. P. McEvoy and G. W. Brudvig, *Chem. Rev.*, 2006, **106**, 4455–4483.
3 D. J. Vinyard, G. M. Ananyev and G. C. Dismukes, *Annu. Rev. Biochem.*, 2013, **82**, 577–606.
4 R. E. Blankenship, *Molecular Mechanisms of Photosynthesis*, Wiley-Blackwell, 2nd edn, 2014.
5 R. Pal, C. F. A. Negre, L. Vogt, R. Pokhrel, M. Z. Ertem, G. W. Brudvig and V. S. Batista, *Biochemistry*, 2013, **52**, 7703–7706.
6 Y. Umena, K. Kawakami, J.-R. Shen and N. Kamiya, *Nature*, 2011, **473**, 55–60.
7 B. Kok, B. Forbush and M. McGloin, *Photochem. Photobiol.*, 1970, **11**, 457–475.
8 B. Forbush, B. Kok and M. P. McGloin, *Photochem. Photobiol.*, 1971, **14**, 307–321.
9 V. Krewald, M. Retegan, N. Cox, J. Messinger, W. Lubitz, S. DeBeer, F. Neese and D. A. Pantazis, *Chem. Sci.*, 2015, **6**, 1676–1695.
10 D. A. Pantazis, W. Ames, N. Cox, W. Lubitz and F. Neese, *Angew. Chem., Int. Ed.*, 2012, **51**, 9935–9940.
11 A. Boussac, M. Sugiura, A. W. Rutherford and P. Dorlet, *J. Am. Chem. Soc.*, 2009, **131**, 5050–5051.
12 N. Cox, M. Retegan, F. Neese, D. A. Pantazis, A. Boussac and W. Lubitz, *Science*, 2014, **345**, 804–808.
13 A. Klauss, M. Haumann and H. Dau, *Proc. Natl. Acad. Sci. U. S. A.*, 2012, **109**, 16035–16040.
14 N. Kamiya and J. R. Shen, *Proc. Natl. Acad. Sci. U. S. A.*, 2003, **100**, 98–103.
15 K. N. Ferreira, T. M. Iverson, K. Maghlaoui, J. Barber and S. Iwata, *Science*, 2004, **303**, 1831–1838.
16 B. Loll, J. Kern, W. Saenger, A. Zouni and J. Biesiadka, *Nature*, 2005, **438**, 1040–1044.
17 A. Guskov, J. Kern, A. Gabdulkhakov, M. Broser, A. Zouni and W. Saenger, *Nat. Struct. Mol. Biol.*, 2009, **16**, 334–342.
18 J. Yano, J. Kern, K. D. Irrgang, M. J. Latimer, U. Bergmann, P. Glatzel, Y. Pushkar, J. Biesiadka, B. Loll, K. Sauer, J. Messinger, A. Zouni and V. K. Yachandra, *Proc. Natl. Acad. Sci. U. S. A.*, 2005, **102**, 12047–12052.
19 A. Grundmeier and H. Dau, *Biochim. Biophys. Acta*, 2012, **1817**, 88–105.
20 K. Sauer, J. Yano and V. K. Yachandra, *Coord. Chem. Rev.*, 2008, **252**, 318–335.
21 P. E. M. Siegbahn, *Chem.–Eur. J.*, 2008, **14**, 8290–8302.
22 R. Neutze, R. Wouts, D. van der Spoel, E. Weckert and J. Hajdu, *Nature*, 2000, **406**, 752–757.
23 H. N. Chapman, P. Fromme, A. Barty, T. A. White, R. A. Kirian, A. Aquila, M. S. Hunter, J. Schulz, D. P. DePonte, U. Weierstall, R. B. Doak, F. R. N. C. Maia, A. V. Martin, I. Schlichting, L. Lomb, N. Coppola, R. L. Shoeman, S. W. Epp, R. Hartmann, D. Rolles, A. Rudenko, L. Foucar, N. Kimmel, G. Weidenspointner, P. Holl, M. Liang, M. Barthelmess, C. Caleman, S. Boutet, M. J. Bogan, J. Krzywinski, C. Bostedt, S. Bajt, L. Gumprecht, B. Rudek, B. Erk, C. Schmidt, A. Homke, C. Reich, D. Pietschner, L. Struder, G. Hauser, H. Gorke, J. Ullrich, S. Herrmann,

G. Schaller, F. Schopper, H. Soltau, K.-U. Kuhnel, M. Messerschmidt, J. D. Bozek, S. P. Hau-Riege, M. Frank, C. Y. Hampton, R. G. Sierra, D. Starodub, G. J. Williams, J. Hajdu, N. Timneanu, M. M. Seibert, J. Andreasson, A. Rocker, O. Jonsson, M. Svenda, S. Stern, K. Nass, R. Andritschke, C.-D. Schroter, F. Krasniqi, M. Bott, K. E. Schmidt, X. Wang, I. Grotjohann, J. M. Holton, T. R. M. Barends, R. Neutze, S. Marchesini, R. Fromme, S. Schorb, D. Rupp, M. Adolph, T. Gorkhover, I. Andersson, H. Hirsemann, G. Potdevin, H. Graafsma, B. Nilsson and J. C. H. Spence, *Nature*, 2011, **470**, 73–77.

24 J. Kern, R. Alonso-Mori, J. Hellmich, R. Tran, J. Hattne, H. Laksmono, C. Glöckner, N. Echols, R. G. Sierra, J. Sellberg, B. Lassalle-Kaiser, R. J. Gildea, P. Glatzel, R. W. Grosse-Kunstleve, M. J. Latimer, T. A. McQueen, D. DiFiore, A. R. Fry, M. Messerschmidt, A. Miahnahri, D. W. Schafer, M. M. Seibert, D. Sokaras, T.-C. Weng, P. H. Zwart, W. E. White, P. D. Adams, M. J. Bogan, S. Boutet, G. J. Williams, J. Messinger, N. K. Sauter, A. Zouni, U. Bergmann, J. Yano and V. K. Yachandra, *Proc. Natl. Acad. Sci. U. S. A.*, 2012, **109**, 9721–9726.

25 J. Kern, R. Alonso-Mori, R. Tran, J. Hattne, R. J. Gildea, N. Echols, C. Glöckner, J. Hellmich, H. Laksmono, R. G. Sierra, B. Lassalle-Kaiser, S. Koroidov, A. Lampe, G. Han, S. Gul, D. DiFiore, D. Milathianaki, A. R. Fry, A. Miahnahri, D. W. Schafer, M. Messerschmidt, M. M. Seibert, J. E. Koglin, D. Sokaras, T.-C. Weng, J. Sellberg, M. J. Latimer, R. W. Grosse-Kunstleve, P. H. Zwart, W. E. White, P. Glatzel, P. D. Adams, M. J. Bogan, G. J. Williams, S. Boutet, J. Messinger, A. Zouni, N. K. Sauter, V. K. Yachandra, U. Bergmann and J. Yano, *Science*, 2013, **340**, 491–495.

26 J. Kern, R. Tran, R. Alonso-Mori, S. Koroidov, N. Echols, J. Hattne, M. Ibrahim, S. Gul, H. Laksmono, R. G. Sierra, R. J. Gildea, G. Han, J. Hellmich, B. Lassalle-Kaiser, R. Chatterjee, A. S. Brewster, C. A. Stan, C. Glöckner, A. Lampe, D. DiFiore, D. Milathianaki, A. R. Fry, M. M. Seibert, J. E. Koglin, E. Gallo, J. Uhlig, D. Sokaras, T.-C. Weng, P. H. Zwart, D. E. Skinner, M. J. Bogan, M. Messerschmidt, P. Glatzel, G. J. Williams, S. Boutet, P. D. Adams, A. Zouni, J. Messinger, N. K. Sauter, U. Bergmann, J. Yano and V. K. Yachandra, *Nat. Commun.*, 2014, **5**, 4371.

27 C. Kupitz, S. Basu, I. Grotjohann, R. Fromme, N. A. Zatsepin, K. N. Rendek, M. S. Hunter, R. L. Shoeman, T. A. White, D. Wang, D. James, J.-H. Yang, D. E. Cobb, B. Reeder, R. G. Sierra, H. Liu, A. Barty, A. L. Aquila, D. Deponte, R. A. Kirian, S. Bari, J. J. Bergkamp, K. R. Beyerlein, M. J. Bogan, C. Caleman, T.-C. Chao, C. E. Conrad, K. M. Davis, H. Fleckenstein, L. Galli, S. P. Hau-Riege, S. Kassemeyer, H. Laksmono, M. Liang, L. Lomb, S. Marchesini, A. V. Martin, M. Messerschmidt, D. Milathianaki, K. Nass, A. Ros, S. Roy-Chowdhury, K. Schmidt, M. Seibert, J. Steinbrener, F. Stellato, L. Yan, C. Yoon, T. A. Moore, A. L. Moore, Y. Pushkar, G. J. Williams, S. Boutet, R. B. Doak, U. Weierstall, M. Frank, H. N. Chapman, J. C. H. Spence and P. Fromme, *Nature*, 2014, **513**, 261–265.

28 M. Askerka, J. Wang, G. W. Brudvig and V. S. Batista, *Biochemistry*, 2014, **53**, 6860–6862.

29 M. Suga, F. Akita, K. Hirata, G. Ueno, H. Murakami, Y. Nakajima, T. Shimizu, K. Yamashita, M. Yamamoto, H. Ago and J.-R. Shen, *Nature*, 2014, **517**, 99–103.

30 M. Askerka, D. J. Vinyard, J. Wang, G. W. Brudvig and V. S. Batista, *Biochemistry*, 2015, **54**, 1713–1716.
31 V. K. Yachandra, K. Sauer and M. P. Klein, *Chem. Rev.*, 1996, **96**, 2927–2950.
32 P. E. M. Siegbahn, *Biochim. Biophys. Acta*, 2013, **1827**, 1003–1019.
33 P. E. M. Siegbahn, *Chem.–Eur. J.*, 2006, **12**, 9217–9227.
34 J. Messinger, M. Badger and T. Wydrzynski, *Proc. Natl. Acad. Sci. U. S. A.*, 1995, **92**, 3209–3213.
35 V. L. Pecoraro, M. J. Baldwin, M. T. Caudle, W.-Y. Hsieh and N. A. Law, *Pure Appl. Chem.*, 1998, **70**, 925–929.
36 G. W. Brudvig, *Philos. Trans. R. Soc., B*, 2008, **363**, 1211–1219.
37 V. A. Szalai, D. A. Stone and G. W. Brudvig, in *Photosynthesis: Mechanisms and Effects*, vol. 2, ed. G. Garab, Kluwer Academic, Dordrecht, The Netherlands, 1998, pp. 1403–1406.
38 S. Romain, L. Vigara and A. Llobet, *Acc. Chem. Res.*, 2009, **42**, 1944–1953.
39 W. Hillier and T. Wydrzynski, *Biochim. Biophys. Acta*, 2001, **1503**, 197–209.
40 W. Hillier and T. Wydrzynski, *Coord. Chem. Rev.*, 2008, **252**, 306–317.
41 W. Hillier and T. Wydrzynski, *Phys. Chem. Chem. Phys.*, 2004, **6**, 4882–4889.
42 M. Lundberg, M. R. A. Blomberg and P. E. M. Siegbahn, *Theor. Chem. Acc.*, 2003, **110**, 130–143.
43 J. A. Dean, *Lange's Handbook of Chemistry*, McGraw Hill Book Co., New York, 1985.
44 J. Burgess, *Ions in Solution: Basic Principles of Chemical Interactions*, Halsted Press, New York, 1988.
45 D. T. Richens, *The Chemistry of Aqua Ions*, Wiley, Chichester, U.K., 1997.
46 Y. Ducommun, K. E. Newman and A. E. Merbach, *Inorg. Chem.*, 1980, **19**, 3696–3703.
47 F. P. Rotzinger, *J. Am. Chem. Soc.*, 1997, **119**, 5230–5238.
48 D. Kuzek and R. J. Pace, *Biochim. Biophys. Acta*, 2001, **1503**, 123–137.
49 R. Tagore, H. Y. Chen, R. H. Crabtree and G. W. Brudvig, *J. Am. Chem. Soc.*, 2006, **128**, 9457–9465.
50 C. W. Cady, K. E. Shinopoulos, R. H. Crabtree and G. W. Brudvig, *Dalton Trans.*, 2010, **39**, 3985–3989.
51 M. T. Caudle and V. L. Pecoraro, *J. Am. Chem. Soc.*, 1997, **119**, 3415–3416.
52 E. M. Sproviero, K. Shinopoulos, J. A. Gascón, J. P. McEvoy, G. W. Brudvig and V. S. Batista, *Philos. Trans. R. Soc., B*, 2008, **363**, 1149–1156.
53 R. Tagore, R. H. Crabtree and G. W. Brudvig, *Inorg. Chem.*, 2007, **46**, 2193–2203.
54 I. L. McConnell, V. M. Grigoryants, C. P. Scholes, W. K. Myers, P.-Y. Chen, J. W. Whittaker and G. W. Brudvig, *J. Am. Chem. Soc.*, 2012, **134**, 1504–1512.
55 M. Amin, L. Vogt, S. Vassiliev, I. Rivalta, M. M. Sultan, D. Bruce, G. W. Brudvig, V. S. Batista and M. R. Gunner, *J. Phys. Chem. B*, 2013, **117**, 6217–6226.
56 W. F. Beck and G. W. Brudvig, *Biochemistry*, 1986, **25**, 6479–6486.
57 P. O. Sandusky and C. F. Yocum, *Biochim. Biophys. Acta*, 1984, **766**, 603–611.
58 P. O. Sandusky and C. F. Yocum, *Biochim. Biophys. Acta*, 1986, **849**, 85–93.
59 W. F. Beck, J. C. de Paula and G. W. Brudvig, *J. Am. Chem. Soc.*, 1986, **108**, 4018–4022.
60 M. Pérez Navarro, W. M. Ames, H. Nilsson, T. Lohmiller, D. A. Pantazis, L. Rapatskiy, M. M. Nowaczyk, F. Neese, A. Boussac, J. Messinger, W. Lubitz and N. Cox, *Proc. Natl. Acad. Sci. U. S. A.*, 2013, **110**, 15561–15566.

61 R. D. Britt, J. L. Zimmermann, K. Sauer and M. P. Klein, *J. Am. Chem. Soc.*, 1989, **111**, 3522–3532.
62 P. H. Oyala, T. A. Stich, R. J. Debus and R. D. Britt, *J. Am. Chem. Soc.*, 2015, **137**, 8829–8837.
63 M. Askerka, D. J. Vinyard, G. W. Brudvig and V. S. Batista, *Biochemistry*, 2015, **54**, 5783–5786.
64 T.-A. Ono and Y. Inoue, *Arch. Biochem. Biophys.*, 1988, **264**, 82–92.
65 D. J. Vinyard and G. W. Brudvig, *Biochemistry*, 2015, **54**, 622–628.
66 H. Nilsson, F. Rappaport, A. Boussac and J. Messinger, *Nat. Commun.*, 2014, **5**, 4305.
67 N. Cox and J. Messinger, *Biochim. Biophys. Acta*, 2013, **1827**, 1020–1030.
68 H. Nilsson, T. Krupnik, J. Kargul and J. Messinger, *Biochim. Biophys. Acta*, 2014, **1837**, 1257–1262.
69 L. Rapatskiy, N. Cox, A. Savitsky, W. M. Ames, J. Sander, M. M. Nowaczyk, M. Rögner, A. Boussac, F. Neese, J. Messinger and W. Lubitz, *J. Am. Chem. Soc.*, 2012, **134**, 16619–16634.
70 A. Klauss, M. Haumann and H. Dau, *J. Phys. Chem. B*, 2015, **119**, 2677–2689.
71 G. Hendry and T. Wydrzynski, *Biochemistry*, 2003, **42**, 6209–6217.
72 *CRC Handbook of Chemistry and Physics*, ed. D. R. Lide, CRC Press/Taylor and Francis, Boca Raton, FL, 88th (Internet Version 2008) edn, 2008.
73 T. Taguchi, R. Gupta, B. Lassalle-Kaiser, D. W. Boyce, V. K. Yachandra, W. B. Tolman, J. Yano, M. P. Hendrich and A. S. Borovik, *J. Am. Chem. Soc.*, 2012, **134**, 1996–1999.
74 R. Gupta, T. Taguchi, B. Lassalle-Kaiser, E. L. Bominaar, J. Yano, M. P. Hendrich and A. S. Borovik, *Proc. Natl. Acad. Sci. U. S. A.*, 2015, **112**, 5319–5324.

